Optimizing Electron–Positron Pair Production on kJ-Class High-Intensity Lasers for the Purpose of Pair-Plasma Creation

Introduction

The creation of a relativistically hot electron–positron plasma in the laboratory is an ambitious experimental challenge that has yet to be realized. Electron–positron pair plasmas are theoretically interesting because of the mass symmetry between the plasma components. For example, this symmetry results in the absence of both acoustic modes and Faraday rotation.[1,2] Waves and instabilities in electron–positron plasmas differ significantly from asymmetric electron–ion plasmas and have been discussed theoretically in Refs. 1 and 2. Electron–positron plasmas are important in astrophysical settings;[3] new insights into astrophysical phenomena such as black holes, pulsar magnetospheres, active galactic nuclei, bipolar outflows (jets), and gamma-ray bursts (GRB) may be gained by appropriate laboratory investigations.[4]

The main difficulty in creating an electron–positron plasma arises because terrestrial positron sources are typically very weak; e.g., source rates of $\sim 10^6$ positrons s^{-1} are obtained using radioactive sources[5,6] and (10^8 to 10^9) positrons s^{-1} using accelerator-based sources.[7] To date, classical single-component, positron-plasma charge clouds have been created and confined, with cloud sizes slightly exceeding the Debye length, by storing and cooling positrons created through radioactive decay in electrostatic Penning traps.[5,6,8] Penning traps cannot, however, simultaneously confine significant numbers of both positive and negative species.[2] In principle, the simultaneous confinement of electrons and positrons in non-neutral stellerators[9] or mirror machines[10] appears possible, but it has yet to be achieved. An alternative to the above schemes is proposed that uses ultra-intense laser pulses as an intense positron source.[11–17] The first step toward producing a pair plasma is to optimize the pair-production rate. Calculations in this article indicate that source rates approaching 10^{24} positrons s^{-1} are attainable with the generation of petawatt laser systems either recently completed, such as OMEGA EP,[18] or currently under construction, e.g., NIF-ARC.[19] Such source rates are shown to be high enough that the density of pairs approaches that required for the formation of a pair plasma.

The following sections of this article (1) present calculations of the direct and indirect yield as a function of laser intensity and target geometry; (2) analyze the results, optimizing the yields, and the production rates; (3) estimate the likelihood of pair–plasma production; and (4) summarize our conclusions.

Calculation of Positron Yield in Laser–Target Interactions

High-energy petawatt lasers, such as LLE's recently completed OMEGA EP Laser Facility,[18] deliver kilojoules of laser energy at focused laser intensities of $I_0 \lesssim 10^{20}$ W/cm^2. Such intensities are still several orders of magnitude below the level required to create electron–positron pairs from the vacuum.[20–22] However, laser–matter interaction at intensities $I_0 \gtrsim 10^{18}$ W/cm^2 efficiently produce hot electrons with characteristic energies in the MeV range,[23] which may be approximated by the ponderomotive (Wilks) scaling for the hot-electron "temperature"[24]

$$\Theta_{\text{hot}} = 0.511\left[\left(1 + I_{18}\lambda_{\mu\text{m}}^2/1.37\right)^{1/2} - 1\right]\text{MeV}, \qquad (1)$$

where I_{18} is the laser intensity in units of 10^{18} W/cm^2 and $\lambda_{\mu\text{m}}$ is the laser wavelength in μm (= 1.053 μm for OMEGA EP). This scaling predicts temperatures ranging from $\Theta_{\text{hot}} \sim 1$ MeV at $I_{\text{L}} = 1 \times 10^{19}$ W/cm^2 to $\Theta_{\text{hot}} \sim 15$ MeV at $I_{\text{L}} = 1 \times 10^{21}$ W/cm^2. Electrons with kinetic energies exceeding the threshold value, $T_{\text{th,e}} \approx 2m_{\text{e}}c^2 = 1.022$ MeV (neglecting the small correction due to recoil of the nucleus), have a finite probability of creating an electron–positron pair in matter. A significant uncertainty exists in the scaling of hot-electron temperature with laser intensity. An alternative scaling, the so-called Beg scaling,[25] has been proposed $\left[\Theta_{\text{hot}} = 0.46\left(I_{19}\lambda_{\mu\text{m}}^2\right)^{1/3}\text{MeV}\right]$, which seems to give better agreement with a certain class of high-contrast experiments.[26] The Beg scaling predicts significantly lower temperatures for a given laser intensity leading to less-favorable pair-production rates.

Several mechanisms lead to the production of pairs: Pairs can be created directly (trident process) by energetic electrons interacting with the Coulomb field of the atomic nucleus (or with the field of an atomic electron) or pairs can be created indirectly.

Indirect production first requires the production of a bremsstrahlung photon followed by pair production by the photon in the nuclear (or atomic-electron) field (photo-pair production). The reaction rate for direct production in the nuclear (electron) field is of the order of $Z^2 n_{\rm hot} n_i \alpha^2$ ($n_{\rm hot} n_{\rm e} \alpha^2$), while bremsstrahlung is of the order of $Z^2 n_{\rm hot} n_i \alpha$ and pair production is $Z^2 n_\gamma n_i \alpha$. Here, $\alpha \approx 1/137$ is the fine-structure constant, Z is the atomic number, and $n_{\rm hot}$, n_i, $n_{\rm e}$, and n_γ are the hot-electron, atomic, atomic-electron, and photon number densities, respectively. Two-photon-pair production is the lowest-order process in α (zeroth), but it can be ignored because the (bremsstrahlung) photon density is orders of magnitude lower than the hot-electron number density. The reverse of this process, pair annihilation, is expected to occur and will provide a characteristic annihilation radiation signature of back-to-back photons at ~511 keV, which can be used to diagnose the presence of pairs.[27,28]

The ratio of the cross sections for direct and photoproduction, with energy dependence, has been given in Ref. 29:

$$\frac{\sigma_T}{\sigma_{\gamma \to e^+e^-}} = \frac{\alpha}{\pi}\left[\log\left(\frac{E_0}{m_e c^2}\right)\log\left(\frac{E_0}{2.137\, m_e c^2 Z^{-1/3}}\right) + \frac{1}{3}\log^2\left(2.137\, Z^{-1/3}\right)\right], \quad (2)$$

where E_0 is the total energy of the incident electron (photons are assumed to have the same energy), $m_{\rm e}$ is the electron mass, and c is the speed of light. From this expression it can be seen that pair production is more efficient (at 5 MeV the ratio is $\sigma_T/\sigma_{\gamma \to e^+e^-} = 0.017$), but there is an additional inefficiency associated with first creating the hard bremsstrahlung photons. In the following subsections, the efficiencies of each process are carefully computed. The cross sections (per atom) for both direct production σ_T and photon-pair production $\sigma_{\gamma \to e^+e^-}$ are proportional to Z^2. The production efficiency will be greatest using a target material that optimizes the product of Z^2 and the atomic number density n_i. In this article we assume the target to be Au ($Z = 79$), which is close to optimal $\left(Z^2 n_i = Z^2 \rho N_{\rm A}/A \sim 3.66 \times 10^{26}\ {\rm cm}^{-3}\right)$, where A is the atomic weight, ρ is the mass density, and $N_{\rm A}$ is the Avogadro number.

The threshold kinetic energy for the production of muons is $T_{{\rm th},\mu} = 212$ MeV and $T_{{\rm th},\pi} \approx 280$ MeV for pions.[30] It is unlikely that muons or pions can be created with any significant efficiency with the current generation of petawatt-class lasers.

1. Direct Pair Production by Electrons (Trident Production)

Trident production[(a),29,31,32] of electron–positron pairs by fast electrons colliding with the Coulomb field of an atomic nucleus has been approximated by either the Bhabha cross section[29] or various forms valid at high energy.[33] The Bhabha cross section is not entirely satisfactory since the uncertainties over the range of electron energies considered here (ranging roughly from threshold to a few tens of MeV) are hard to determine.[11] More recently Gryaznykh[34] numerically evaluated the integrals arising from the three lowest-order diagrams that have been computed by Baĭer *et al.*[35] Reference 34 provides a fitting formula for the total cross section σ_T, which is valid from threshold to ~100 MeV,

$$\sigma_T = 5.22\, Z^2 \log^3\left[\frac{2.30 + T_0({\rm MeV})}{3.52}\right]\mu{\rm b}, \quad (3)$$

together with limiting forms near threshold

$$\sigma_T = \frac{7\, Z^2 r_0^2 \alpha^2}{2304}\,\frac{\left(T_0 - 2m_e c^2\right)^3}{\left(m_e c\right)^3}, \quad (4)$$

and at high energies

$$\sigma_T = \frac{28\pi Z^2 r_0^2 \alpha^2}{27}\log^3\left(\frac{T_0}{m_e c^2}\right). \quad (5)$$

Here, T_0 is the kinetic energy of the incident electron, $r_0 \equiv e^2/m_e c^2 = 2.82 \times 10^{-13}$ cm^2 is the classical electron radius, and e is the elementary charge. In an infinite target, the trident yield $Y_{+,T}$ can be computed for a given probability distribution of incident electron kinetic energies, $f_0(T_0)$, by integrating along the electron path, running down in kinetic energy from the initial value T_0 assuming the continuous slowing-down approximation (CSDA),

$$Y_{+,T} = \eta_r N_{\rm e}\int_0^\infty {\rm d}T_0 f_0(T_0)\int_0^{T_0} {\rm d}T n_i \sigma_T(T)\left|\frac{{\rm d}T}{{\rm d}s}\right|^{-1} = \eta_r N_{\rm e}\int_0^\infty {\rm d}T_0 f_0(T_0)\int_0^{s(T_0)} {\rm d}s' n_i \sigma_T\left[T(T_0, s')\right]. \quad (6)$$

[(a)] In general, "trident" and "quartets" refer to the production of lepton pairs by virtual photons in the Coulomb fields of nuclei and atomic electrons, respectively. "Pairs" and "triplets" refer to the corresponding process induced by real photons.

Here N_e is the total number of hot electrons, s' is the path length variable for an electron of initial kinetic energy T_0 of CSDA range $s(T_0)$, and $\eta_r = 1$. The yield in a thin target, significantly thinner than the hot-electron practical range, can be estimated by introducing the "refluxing efficiency" $\eta_r \lesssim 1$ (Ref. 36). The refluxing efficiency represents the fraction of hot electrons that are trapped by the space charge of the target relative to the total number, which can be close to unity for a range of target interaction conditions.[36,37] The electron stopping power $-(\mathrm{d}T/\mathrm{d}s)$, from which $T(T_0,s) = T_0 + \int_0^s \mathrm{d}s'\left(\mathrm{d}T/\mathrm{d}s'\right)$ is computed, has been taken from Ref. 38.

The yield computed according to Eq. (6), per kJ of hot electrons, is shown as the dashed line in Fig. 116.1 for a range of hot-electron temperatures, perfect refluxing efficiency $\eta_r = 1$, and an exponential hot-electron energy distribution function $f_0(T_0) = \left(1/\Theta_{\mathrm{hot}}\right)\exp\left(-T_0/\Theta_{\mathrm{hot}}\right)$. The average positron kinetic energy $\overline{T}_+$ for an incident electron of energy T_0 is calculated by the formula $\overline{T}_+ = T_0\left\{1/3 - b\,\log\left[T_0/\left(3m_ec^2\right)\right]\right\}$. The dimensionless parameter b (= 0.0565) has been found in Ref. 34 by fitting to the results of numerical computation of the integrals. The average positron energy produced for a distribution of hot electrons, $f_0(T_0)$, can be estimated by

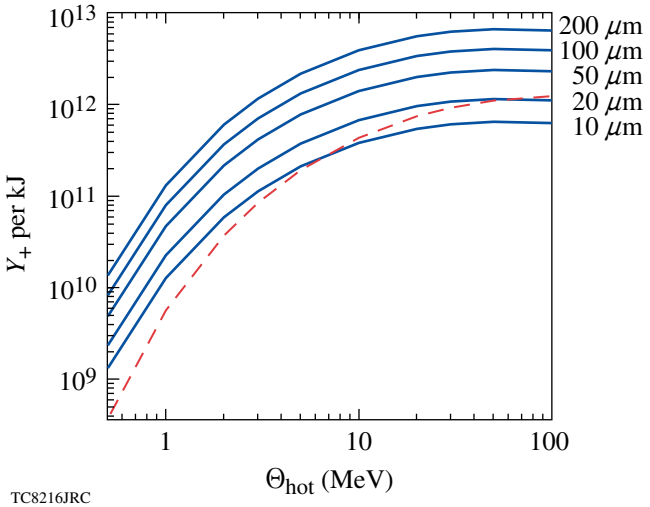

Figure 116.1
The solid curves show the photo-produced positron yield (number of pairs per kJ of hot electrons) as a function of hot-electron temperature (in MeV) for targets of thickness ranging from 10 μm to 200 μm. The dashed curve shows the direct (trident) yield from Eq. (6).

$$\left\langle T_{+/}\right\rangle_T = \int_0^\infty \mathrm{d}T_0 f_0(T_0)\frac{1}{\Xi(T_0)} \times \int_0^{s(T_0)} \mathrm{d}s'\,\overline{T}_+\left[T(T_0,s')\right]\sigma_T\left[T(T_0,s')\right], \tag{7}$$

where $\Xi(T_0) \equiv \int_0^{s(T_0)} \mathrm{d}s'\,\sigma_T$.

2. Indirect Photo-Pair Production

a. Hard x-ray production. To compute the indirect yield, one must first calculate the hard component of the bremsstrahlung. This can be estimated using the Bethe–Heitler cross section[39]

$$\sigma_\gamma(E_0,k)\mathrm{d}k = Z^2 r_0^2 \alpha \frac{\mathrm{d}k}{kE_0^2}\left\{\left(E_0^2+E^2\right)\left[\phi_1(\gamma) - \frac{4}{3}\log Z\right] - \frac{2}{3}EE_0\left[\phi_2(\gamma) - \frac{4}{3}\log Z\right]\right\}. \tag{8}$$

This represents the cross section for an incident electron of total energy $E_0 = (T_0 + m_ec^2)$ to produce a bremsstrahlung photon, in the field of an atomic nucleus, with energy between k and $k + \mathrm{d}k$ (the scattered electron has energy $E = E_0 - k$). The screening factors $\phi_1(\gamma)$ and $\phi_2(\gamma)$ have their usual definitions,[40] with the screening parameter γ given by $\gamma = 100\,m_ec^2k/\left(E_0EZ^{1/3}\right)$.

The photon energy spectrum, differential in photon energy, produced by electrons with an initial energy spectrum $f_0(T_0)$ that run down their energy completely in the target is given by

$$N_\gamma(k)\mathrm{d}k = \left(\eta_r N_e\right)\int_0^\infty \mathrm{d}T_0 f_0(T_0) \times \int_0^{T_0} \mathrm{d}T n_i \sigma_\gamma(E,k)\mathrm{d}k\left|\frac{\mathrm{d}T}{\mathrm{d}s}\right|^{-1} = \left(\eta_r N_e\right)\int_0^\infty \mathrm{d}T_0 f_0(T_0) \times \int_0^{s(T_0)} \mathrm{d}s'\,n_i\sigma_\gamma\left[E(E_0,s')k\right]\mathrm{d}k. \tag{9}$$

The energy contained in bremsstrahlung photons, ϵ_γ, may be computed by multiplying Eq. (9) by photon energy k and integrating, to give

$$\epsilon_{\gamma\{0,>\}} = (\eta_r N_e)\int_0^\infty dT_0 f_0(T_0) T_0 Y_{\{0,>\}}(T_0), \qquad (10)$$

where $Y_{\{0,>\}}$ has the definition

$$Y_{\{0,>\}}(T_0) \equiv \frac{n_i}{T_0}\int_{\{0,2mc^2\}}^\infty dk k \sigma_\gamma\left[E(T_0,s')k\right]. \qquad (11)$$

In the above definitions of ϵ_γ and Y, the symbol "0" or ">" in the subscript indicates if the photon energy k in the k integration is either unrestricted or restricted to be greater than the threshold for pair production, $k > 2m_e c^2$ (= 1.022 MeV), respectively. The quantity Y_0 is the usual "radiation yield."[38] This is the fraction of an incident electron's kinetic energy T_0 that is converted into radiation as the electron thermalizes within an infinite medium of a given material. Likewise, $Y_>$ measures the fraction of this energy that is above threshold for pair production. For convenience, the "bremsstrahlung efficiency" $\eta_{\gamma,\{0,>\}} \equiv \epsilon_{\gamma,\{0,>\}}/(N_e \Theta_{hot})$ has been introduced. It is defined as the ratio of bremsstrahlung energy to hot-electron kinetic energy for hot electrons described by the probability distribution $f_0(T_0)$.

Figure 116.2 shows a plot of the bremsstrahlung efficiency $\eta_{\gamma,0}$, radiation yield Y_0, and a comparison with the Koch and Motz scaling,[39]

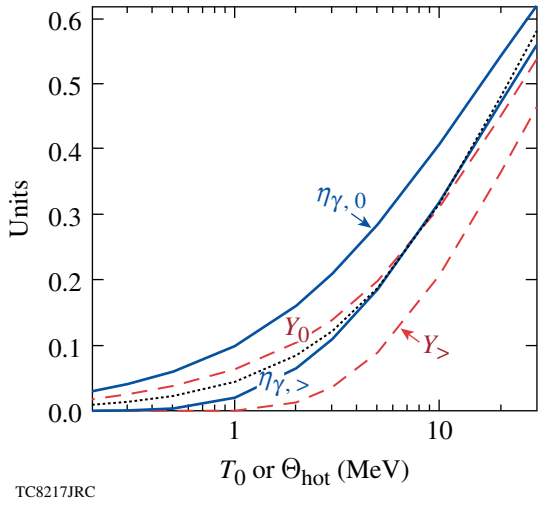

Figure 116.2
Solid curves show the bremsstrahlung efficiency $\eta_{\gamma,0} \equiv \epsilon_{\gamma,0}/(N_e\Theta_{hot})$ and bremsstrahlung efficiency above threshold $\eta_{\gamma,>}$ as functions of hot-electron temperature from Eq. (10). The dashed curves show the radiation yield Y_0 and radiation yield above threshold $Y_>$ [Eq. (11)] as functions of electron kinetic energy. The dotted curve is the Koch and Motz thick-target bremsstrahlung scaling.[39]

$$(Y_0)_{K-M} = 3\times10^{-4} Z\mathcal{T}_0'/\left(1+3\times10^{-4} Z\mathcal{T}_0'\right),$$

where $\mathcal{T}_0'$ is the electron kinetic energy in mass units, $\mathcal{T}_0' \equiv T_0/m_e c^2$. The quantities $\eta_{\gamma,>}$ and $Y_>$ are also shown. In these calculations the best-available tabulated differential bremsstrahlung cross sections have been used (from Ref. 41) rather than the Bethe–Heitler expression [Eq. (8)].

Two important loss mechanisms preclude the *extraction* of an amount of bremsstrahlung energy equal to the radiation yield in practical laser–foil interaction experiments. These are (a) the escape of high-energy electrons from the foil (i.e., $\eta_r < 1$) and (b) the self-absorption of a portion of the bremsstrahlung generated in the foil. In this application, however, self-absorption is desired—the dominant contribution to the attenuation coefficient being pair production for photon energies ≳5 MeV (Ref. 42). High refluxing efficiency $\eta_r \sim 1$ is observed in experiments conducted at laser energies $E_L \sim 500$ J (Refs. 37 and 43). Future experiments are planned to test the extrapolation to kJ laser energies.[37] Another potentially important consideration for higher target energy densities is target expansion caused by the hot-electron pressure.[44] This represents an additional energy sink for the hot electrons.

b. Pair production. If the bremsstrahlung energy spectrum $N_\gamma(k)$ is known, either experimentally[23] or as computed by Eq. (9), the resulting photo-pair yield is readily computed assuming isotropy and homogeneity of the bremsstrahlung emission. In a foil where Compton scattering is negligible, the number of photo-produced positrons in the (total) energy range $E_+ + dE_+$, produced in a foil of thickness d, is given by

$$N_e + (E_+)dE_+ = \frac{N_A}{A}\int_0^\infty dk \int d\Omega \left(\int_0^d \rho dt \left\{\int_0^t ds \frac{1}{|\cos\theta|}\right.\right.$$
$$\times n_\gamma^-(k,t,\theta)\exp\left[-\mu(k)\frac{(t-s)}{|\cos\theta|}\right]$$
$$\left.\left. + \int_t^d ds \frac{1}{|\cos\theta|} n_\gamma^+(k,t,\theta)\right.\right.$$
$$\left.\left.\times \exp\left[-\mu(k)\frac{(s-t)}{|\cos\theta|}\right]\right\}\right)$$
$$\times \sigma_{\gamma\to e^+e^-}(k,E_+)dE_+, \qquad (12)$$

where E_+ is the (total) positron energy and $\mu(k) = n_i\sigma_{\rm tot}(k)$ is the linear attenuation coefficient for x rays of energy k.[b] The total cross section $\sigma_{\rm tot}$ has contributions from coherent and incoherent Compton scattering, photo-electric absorption, pair production, and photo-nuclear absorption, $\sigma_{\rm tot} = \sigma_{\rm scat} + \sigma_{p-{\rm e}} + \sigma_{\gamma\to{\rm e}^+{\rm e}^-} + \sigma_{p-{\rm n}}$. For photon energies $k \gtrsim 5$ MeV, pair production dominates, while close to threshold, $k \sim 1$ MeV, pair production competes with Compton scattering, $\sigma_{\gamma\to{\rm e}^+{\rm e}^-} \sim \sigma_{\rm scat}$. In gold at solid density, the Compton-scattering cross section $\sigma_{\rm scat} \lesssim 10$ barns translates into a probability of ~0.06 scattering events mm^{-1}. Since it will be verified *a posteriori* that optimal target thicknesses will not exceed the millimeter scale, the assumptions leading to Eq. (12) are justified. In Eq. (12), a new quantity $n_\gamma^\pm(k,t,\theta){\rm d}k{\rm d}t{\rm d}\Omega$, has been introduced. It represents the number of photons of energy between k and $k + {\rm d}k$ that are born with a propagation direction falling into the solid angle between Ω and $\Omega + {\rm d}\Omega$, originating at a depth between t and $t + {\rm d}t$ in the target, and propagating in the forward/backward (+/–) direction. The simplifying assumption that bremsstrahlung photons are isotropic and produced homogeneously throughout the foil volume, perhaps as a result of hot-electron refluxing,[37,43] allows $n_\gamma^\pm$ to be written simply in terms of $N_\gamma(k)$, i.e.,

$$n_\gamma^\pm(k,t,\theta){\rm d}k{\rm d}t{\rm d}\Omega = \frac{1}{2}N_\gamma(k){\rm d}k\left(\frac{{\rm d}t}{d}\right)\left(\frac{{\rm d}\Omega}{2\pi}\right)H[\pm\cos(\theta)],$$

where H is the Heaviside step function. Equation (12) becomes

$$N_{{\rm e}^+}(E_+)dE_+ = \frac{N_{\rm A}}{A}\int_0^\infty {\rm d}kN_\gamma(k)\sigma_{\gamma\to{\rm e}^+{\rm e}^-}(k,E_+)dE_+ \times \int\frac{d\Omega}{4\pi}(\rho L)_{\rm eff}\,, \tag{13}$$

where $(\rho L)_{\rm eff}$ is an "effective depth" in the target (in g/cm^2) for photons of energy k with birth angle θ. This can be written as the product of the average depth in the absence of attenuation, $\rho d/(2|\cos\theta|)$, and an attenuation correcting factor C,

$$(\rho L)_{\rm eff} = \frac{\rho d}{2|\cos\theta|}\cdot C\left[\frac{\mu(k)d}{|\cos\theta|}\right], \tag{14}$$

where $C(w) = 2/w^2\,[\exp(-w)-(1-w)]$. This correction factor ranges from unity, when attenuation along the path w is small, to $C \sim 2|\cos\theta|/(\mu d)$ when the attenuation is large, giving $(\rho L)_{\rm eff} \approx \rho/\mu$.

For solid-density gold, $\rho/\mu = (19.3)(0.79) = 15.3$ g/cm^2 at threshold photon energy ($k = 1.022$ MeV). The angle-average effective depth for photons of energy k required by Eq. (13) becomes

$$\langle\rho L\rangle_\Omega \equiv \frac{1}{4\pi}\int{\rm d}\Omega(\rho L)_{\rm eff} \tag{15}$$

$$= \rho d\int_0^1 {\rm d}x\,\min\left\{\frac{1}{2x}C\left(\frac{\mu d}{x}\right),\frac{r}{d}\right\}. \tag{16}$$

The replacement of $(\rho L)_{\rm eff}$ by $(\rho L)_{\rm eff} \longrightarrow \min\{(\rho L)_{\rm eff}, \rho r\}$ takes into account the effect of finite target radius r (transverse dimensions). The integral in Eq. (16) can be readily performed, yielding

$$\langle\rho L\rangle_\Omega = \frac{1}{2}\frac{\rho}{\mu}\left[1+\left(1-\frac{1}{\mu d}\right)\left(1-e^{-\mu d}\right)-\mu d\,Ei(-\mu d)\right] - \frac{x^*}{2}\frac{\rho}{\mu}\left[1+\left(1-\frac{x^*}{\mu d}\right)\left(1-e^{-\mu d/x^*}\right)-\frac{\mu d}{x^*} \times Ei\left(-\frac{\mu d}{x^*}\right)\right]+x^*\rho r, \tag{17}$$

where $Ei(x)$ is the "exponential integral"[45] and x^* is given by the solution to $x^*/(\mu d)\left(1-e^{-\mu d/x^*}\right) = 1x^*\mu r$, if $r < 1/\mu$, or $x^* = 0$ otherwise. In the case of most interest to experiment, that of weak attenuation $d < r \ll 1/\mu$, Eq. (17) can be approximated as

$$\langle\rho L\rangle_\Omega \approx \frac{\rho d}{2}\log\left(\frac{2.516}{\mu d}\right), \quad \mu d \ll 1, \mu r \geq 1 \tag{18}$$

$$\langle\rho L\rangle_\Omega \approx \frac{\rho d}{2}\log\left(5.437\frac{r}{d}\right), \quad \mu d \ll 1, \mu r \ll 1 \tag{19}$$

In the case of strong attenuation, Eq. (17) can be approximated as

$$\langle\rho L\rangle_\Omega \approx \frac{\rho}{\mu}, \quad \mu d \gg 1, r > d/2. \tag{20}$$

Intermediate cases $\mu d \lesssim 1$ and $\mu r \lesssim 1$ require the numerical evaluation of Eq. (17). The origin of the logarithmic dependence on either foil radius r or absorption $1/\mu$ in Eqs. (18) and (19) is because these serve to regularize the otherwise logarithmically divergent integral, Eq. (16).

[b] Usually called the mass attenuation coefficient when expressed in cm^2/g.

With the above results, the positron energy spectrum is given by

$$N_{e^+}(E_+)dE_+ = \frac{N_A}{A}\int_0^\infty dk N_\gamma(k) \times \sigma_{\gamma \to e^+e^-}(k,E_+)dE_+\langle \rho L\rangle_\Omega , \quad (21)$$

and the total photo-produced positron yield is given by $Y_{+,\gamma} = \int_{mc^2}^{\infty} N_{e^+}(E_+)dE_+$. The yield can be computed directly from the *total* pair cross section

$$\sigma_{\gamma \to e^+e^-}(k) = \int dE_+ \sigma_{\gamma \to e^+e^-}(k,E_+),$$

(the tabulated total cross section is more readily available) according to

$$Y_{+,\gamma} = \frac{N_A}{A}\int_0^\infty dk N_\gamma(k)\sigma_{\gamma \to e^+e^-}(k)\langle \rho L\rangle_\Omega . \quad (22)$$

In Eq. (21), the bremsstrahlung spectrum $N_\gamma(k)$ is given by Eq. (9) and the angle-average effective depth $\langle \rho L\rangle_\Omega$ by Eq. (17), while the differential pair cross-section[41] $\sigma_{\gamma \to e^+e^-}(k,E_+)$ is obtained from the bremsstrahlung cross section [Eq. (8)]. This is achieved by making the substitution $E_0 \longrightarrow -E_+$, $E \longrightarrow E_-$, $k \longrightarrow -k$ and multiplying by $E_+^2 dE_+ / (k^2 dk)$ to take care of the change in density of final states (general substitution rule[46]), where E_- is the energy of the pair electron. In general, this expression for the cross section is accurate only for high energies, so we normalize this differential expression to yield a total cross section $\sigma_{\gamma \to e^+e^-}(k)$ that agrees with those tabulated by Hubbell *et al.*[42] The total cross sections of Hubbell *et al.* represent the most-recent systematic computations and tabulations. The same reference provides the mass attenuation coefficient.

Analysis of the Positron-Yield Calculations

1. Dependence of Positron Yield and Positron Spectrum on Interaction Conditions

Figure 116.1 shows the photo-produced positron yield $Y_{+,\gamma}$ per kilojoule of hot-electron energy as a function of hot-electron temperature for foil thicknesses ranging between 10 μm and 200 μm and a radius r = 1 mm. Photo-produced pairs dominate over trident pairs for targets of thickness $d \gtrsim 20$ μm for hot-electron temperatures $0.5 \lesssim \Theta_{hot} \lesssim 100$ MeV. For pair production in "showers,"[30] it is known that production by virtual photons becomes negligible compared with production by real photons if the target thickness is much more than 1/25 of a radiation length (i.e., for $d \gtrsim 135$ μm in Au). Hot-electron refluxing is responsible for the dominance of photo-produced pairs in thinner-than-expected targets. Refluxing leads to higher photon production for a given foil thickness, i.e., it is the difference between thin- and thick-target bremsstrahlung yields.[37,43]

Figure 116.3 shows the average positron kinetic energy $\langle T_+\rangle_\gamma$ and the average hot-electron kinetic energy Θ_{hot} as a function of laser intensity I_L. In Fig. 116.3, the hot-electron temperature corresponding to a particular laser intensity has been determined by two different scalings: the ponderomotive scaling [Eq. (1)] and the Beg intensity scaling.[25] Unlike transformed Eq. (8), the cross section $\sigma_{\gamma \to e^+e^-}$ is asymmetric in the energy distribution of the pair for high-Z elements near threshold.[40] Accounting for this effect would lead to a slightly higher positron temperature by an amount of the order of the binding energy, which is considered to be negligible.

For a fixed target thickness, the pair creation efficiency (Fig. 116.1) increases with hot-electron temperature, with energetic efficiencies of $E_{e^+}/E_{hot} \sim 1.6 \times 10^{-4}$ achieved for $\Theta_{hot} \sim$ 2 MeV. The optimal hot-electron temperature for the creation of pairs by the Bethe–Heitler process is $(\Theta_{hot})_{opt} \approx 50$ MeV, corresponding to an optimal laser intensity of $(I_L)_{opt} \sim 10^{22}$ W/cm^2, based on the ponderomotive scaling, or $(I_L)_{opt} \sim 10^{25}$ W/cm^2 for the Beg scaling. This enormous variation in optimal laser intensity reflects the degree of uncertainty of the hot-electron temperature scaling with laser intensity in the regime $I_L \gtrsim 10^{21}$ W/cm^2. The

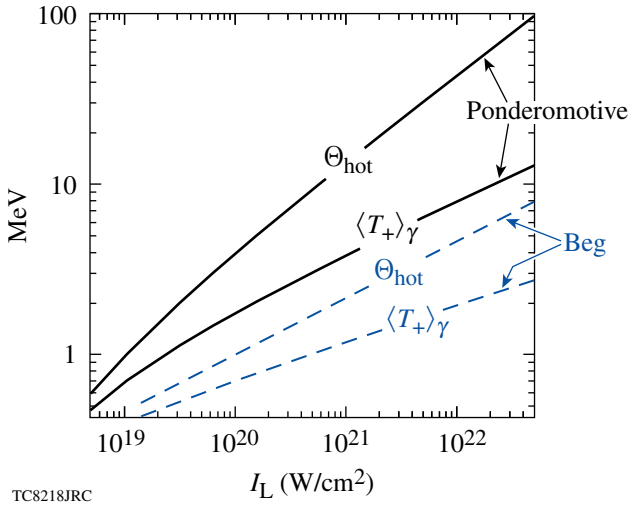

Figure 116.3
The solid curves show the hot-electron temperature (upper curve) and mean positron kinetic energy $\langle T_+\rangle_\gamma$ (lower curve), resulting from the energy spectrum computed in Eq. (21) as functions of laser intensity, assuming the ponderomotive scaling. The dashed curves show the same quantities, but for Beg intensity scaling.

scalings used in Fig. 116.3 have been extrapolated beyond the tested regime $10^{18} \lesssim I_L \lesssim 10^{21}$ W/cm^2. The Beg scaling, which predicts far fewer energetic electrons, was originally based on experiments in the intensity range $I_L \lesssim 10^{19}$ W/cm^2 (Ref. 25). For higher hot-electron temperatures $\Theta_{hot} \gtrsim 50$ MeV, the positron production efficiency $Y_{+,\gamma}$, expressed per kJ of hot-electron energy, decreases ($E_{hot} = N_e \Theta_{hot}$ is the energy content of the hot electrons) because the bremsstrahlung spectrum becomes too hard. The pair-production cross section has a very weak energy dependence above photon energies of $k \sim 10$ MeV, and, as far as maximizing the number of pairs is concerned, it is more efficient to have two photons at half the energy.

For a given laser intensity and small x-ray attenuation μd, the production efficiency increases with target thickness by Eq. (18) or Eq. (19), depending on the ratio of the target radius to the photon linear attenuation length μr. For $\mu d \gg 1$, the efficiency is independent of target thickness and $Y_{+,\gamma} \approx \rho/\mu \int dk N_\gamma(k)\, \sigma_{\gamma \to e^+e^-}(k)$. The attenuation length varies weakly over the photon energy range of $1 < k < 100$ MeV and has the approximate value $1/\mu \leq 0.8$ cm.

2. Optimized Useful Positron Yield

The long-term goal of this work is to create a pair plasma in the space surrounding the foil target where one can conduct experiments, and not in its interior. The "useful" pair yield (i.e., the number of pairs able to escape the target per kJ of hot-electron energy) must therefore be optimized. For a given laser intensity it might seem that the target should be made as thick as possible, up to an x-ray attenuation length $d \sim 1/\mu \sim 0.8$ cm. The target thickness is more tightly constrained, however, since only positrons within a range $r_0(E_+)$ of the surface will be able to escape and the positron range is typically much less than the x-ray attenuation length $r_0 \ll 1/\mu$. The optimal target thickness $d = d_{opt}(\langle T_+ \rangle)$ is a function of the positron energy, determined by the hot-electron spectrum and depends on the scaling of the hot-electron temperature with laser intensity. Unfortunately, the latter represents a source of considerable uncertainty because such scalings are imprecisely known and are extrapolated from significantly smaller laser systems $E_L \lesssim 500$ J.

Figure 116.4 shows an estimate for the optimal target thickness d_{opt} as a function of average positron energy $\langle T_+ \rangle$. Taken with Fig. 116.3, Fig. 116.4 allows one to estimate the optimal target thickness to be made for a given incident laser intensity. This estimate has been obtained by setting the target thickness d equal to the thickness that is known, experimentally, to transmit only 50% of a normally incident monoenergetic electron beam of energy T, where T is set to the average positron energy $T = \langle T_+ \rangle$. This thickness is substantially less than the CSDA range due to the path-length straggling caused by multiple scattering of electrons (and positrons) in the Coulomb field of high-Z nuclei (such as Au). This calculation provides a useful "rule of thumb" that will be refined by future detailed Monte Carlo modeling for a more-precise optimization. For a given thickness d, the transmission Tr(T,Z,d) is computed from the "empirical transmission equation" $\mathrm{Tr}(T,Z,d) = \exp\left[-\alpha\left(d/R_{ex}\right)^{\beta}\right]$ of Ebert *et al.*,[47] where T is the incident electron energy (the differences between electron and positron stopping and scattering in matter are neglected). The "extrapolated range" R_{ex} is approximated by $R_{ex} = 0.565\ [125/(Z + 112)]\ T - 0.423\ [175/(Z + 162)]$ g/cm^2, where $\alpha = (1–1/\beta)^{1-\beta}$ and the parameter β is given by $\beta = [387\ T/Z\ (1 + 7.5 \times 10^{-5}\ ZT^2)]^{0.25}$, with T in MeV. The regime of validity for this expression for Tr(T,Z,d) has been expanded from 4 MeV < T < 12 MeV (Ref. 47) to $T \sim$ 0.25 MeV by using the extrapolated ranges of Tabata *et al.*[48] in the regime 0.25 MeV < T < 4 MeV.

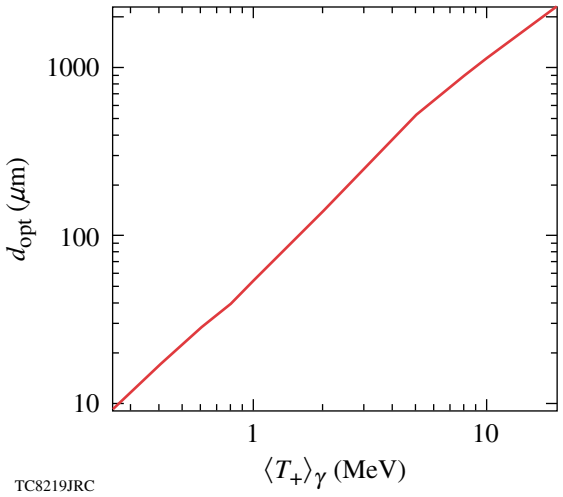

Figure 116.4
The solid curve shows an estimate for the optimal target thickness d_{opt} in μm as a function of average positron energy $\langle T_+ \rangle$ in MeV (positron energy is shown as a function of incident laser intensity in Fig. 116.3).

Figure 116.5 shows the "optimized useful yield" as a function of laser intensity for both Beg and ponderomotive scalings. It is apparent that at intensities of $I_L \sim 5 \times 10^{19}$ W/cm^2,[(c)] there is an uncertainty in the pair yield of almost two orders of magnitude. This is a result of the strong temperature dependence of the yield for electron temperatures close to the threshold

[(c)]Multikilojoule pulses have not been achieved at higher intensity.

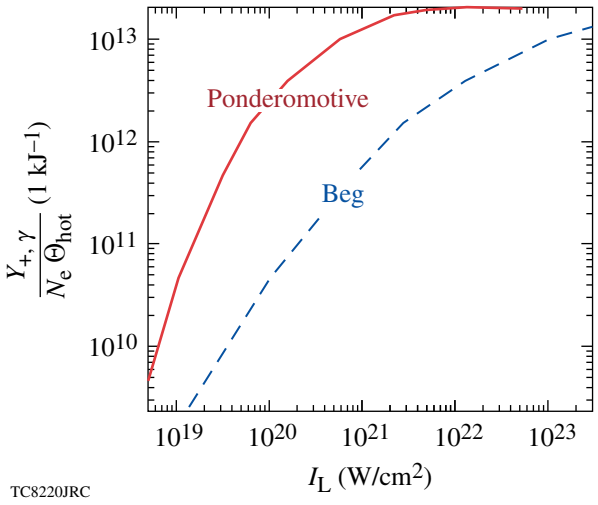

Figure 116.5
The solid curve shows the optimum pair yield per kJ of hot electrons $Y_{+,\gamma}/(N_e\Theta_{hot})$ as a function of incident laser intensity I_L, assuming ponderomotive scaling. The dashed curve shows the same quantity, but for Beg intensity scaling.

for pair production, $\Theta_{hot} \sim 1$ MeV, and the current uncertainty in hot-electron energy scaling with laser intensity. At $I_L = 5 \times 10^{19}$ W/cm^2, the Beg scaling predicts a hot-electron temperature of $\Theta_{hot} \approx 0.8$ MeV and an optimized yield of $Y_{+,\gamma} = 1.5 \times 10^{10}$ pairs per kJ of hot electrons, achieved with a foil of thickness $d = 40$ μm. At the same laser intensity, the ponderomotive scaling predicts $T_{hot} = 2.5$ MeV and a yield of $Y_{+,\gamma} = 1 \times 10^{12}$ per kJ at $d = 200$ μm. This extreme sensitivity will make measurements of the pair yield a good diagnostic for hot-electron temperature in the regime of importance for advanced inertial confinement fusion (ICF) designs, such as fast ignition.[49,50]

A reasonable upper bound for the optimized pair yield on OMEGA EP, and similar future laser systems, can be determined: Assuming the ponderomotive scaling [Eq. (1)], which is more consistent with experiments with significant preplasma,[26] a laser energy of $E_L = 2.5$ kJ delivered at an intensity of $I_L = 5 \times 10^{19}$ W/cm^2, a hot-electron conversion efficiency of $\eta_{L\to e} = 0.2$ (Ref. 51), and perfect refluxing efficiency $\eta_r = 1$ (Refs. 37, 43, and 51), the expected yield is $Y_{+,\gamma} = 5 \times 10^{11}$ pairs. This corresponds to 0.4×10^{10} pairs per steradian, assuming isotropic emission.

3. Optimized Pair-Production rates

The pair-production rate $\dot{Y}_{+,\gamma}$ is estimated by $\dot{Y}_{+,\gamma} \approx Y_{+,\gamma}/\tau^*$, where τ^* is the characteristic production time. Here, τ^* is the time required for the initial hot-electron distribution $f_0(T)$ to slow down so that the relative fraction of particles above threshold,

$$\phi_>(t) \equiv \int_{T_{th,e}}^{\infty} dT\, f(T,t) \Big/ \int_{T_{th,e}}^{\infty} dT\, f_0(T),$$

has fallen by $1/e$, i.e., $\phi_>(\tau^*) = 1/e$. The slowing-down distribution at time t, $f(T,t)$ is computed according to the CSDA approximation: $f(T,t) = f_0(T + \Delta T)$, where $\Delta T = -c\int_{t_0}^{t} dt\beta(T)\left|dt/ds\right|$, $\beta = (1-1/\gamma^2)^{1/2}$, and $\gamma = 1 + T/(m_e c^2)$. This assumes that the production time τ^* is longer than the laser pulse duration. If this is not the case, it must be factored into the calculation.

Figure 116.6 shows the pair-production rate $\dot{Y}_{+,\gamma}$ as a function of laser intensity, for both Beg and ponderomotive scalings. For the case of ponderomotive scaling, the production rate rises rapidly for intensities around $I_L \sim 1 \times 10^{19}$ W/cm^2 ($\Theta_{hot} = 0.96$ MeV) and reaches a maximum at $(I_L)_{max} = 1.5 \times 10^{21}$ W/cm^2 ($\Theta_{hot} = 16.4$ MeV). The maximum-achievable production rate of $\dot{Y}_{+,\gamma} \approx 10^{24}\,\mathrm{s}^{-1}\,\mathrm{kJ}^{-1}$ greatly exceeds any known terrestrial source; indeed, such a high rate is normally encountered only in astrophysical and cosmological settings.[3]

The maximum in pair-production rate is very broad, with 50% of the maximum value achieved at the moderate intensity of $I_L = 1 \times 10^{20}$ W/cm^2 ($\Theta_{hot} = 3.9$ MeV). This implies that highly useful experiments can be conducted at $I_L \ll (I_L)$max. High production rates can be obtained by virtue of the large available energy $E_L \sim 5$ kJ on currently available systems (OMEGA EP) with the practical possibility of high-intensity short-pulse lasers with $E_L \sim 100$ kJ in the near future (e.g., the

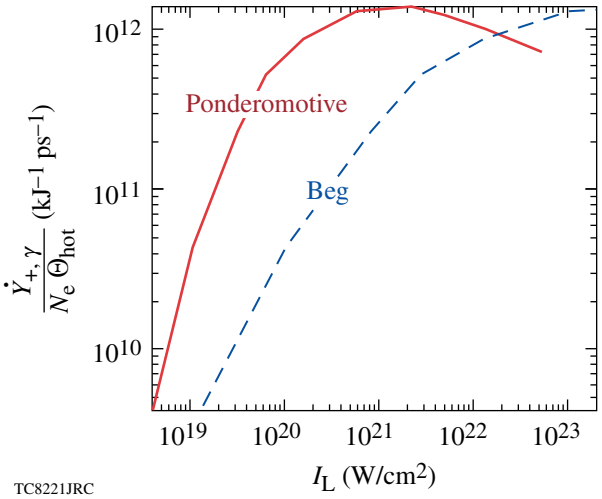

Figure 116.6
The solid curve shows the optimized pair-production rate per kJ of hot electrons $\dot{Y}_{+,\gamma}/(N_e\Theta_{hot})$ as a function of laser intensity for the ponderomotive scaling. The dashed curve shows the same quantity for the Beg intensity scaling.

proposed "HiPER" facility[52,53]). The corresponding intensities for Beg scaling are easily obtained from ponderomotive intensities by making the approximate transformation

$$(I_{20})_{\text{Beg}} \approx 87.9(I_{20})_{\text{pond}}^{3/2} \times \left[1 - 0.35(I_{20})_{\text{pond}}^{-1/2} + 0.08(I_{20})_{\text{pond}}^{-1} - ...\right],$$

which is useful for $(I_{20})_{\text{pond}} \gtrsim 1$. Here, I_{20} is the laser intensity I_{L} expressed in units of 10^{20} W/cm^2.

4. Relativistic Pair-Plasma Production

As shown in Fig. 116.3, the expanding cloud of pair particles will have a temperature characteristic of the hot electrons and γ rays that created it. Unless confined, the relativistic electron–positron pairs will expand into the space surrounding the target at approximately the speed of light.

Although, in general, the expansion into the vacuum can be expected to be quite complicated,[(d)] the expected plasma parameters can be estimated by assuming free expansion at the speed of light from an infinitesimal source, starting at time $t = 0$, combined with a constant source rate $\dot{Y}_{+,\gamma}$. On this basis, the positron density n_+ at radius r and time t is

$$n_+(r,t) = \frac{1}{4\pi r^2}\frac{\dot{Y}_{+,\gamma}}{c} \quad \text{for } c(t-\tau^*) < r < ct; \tag{23}$$

$$\text{otherwise,} \quad n_+(r,t) = 0. \tag{24}$$

This gives in practical units

$$n_+(r,t) \approx 0.7 \times 10^{16}\left(\frac{0.03\text{ cm}}{r}\right)^2 \times \frac{\dot{Y}_{+,\gamma}}{10^{12}\text{ kJ}^{-1}\text{ ps}^{-1}}\frac{E_{\text{hot}}}{2.5\text{ kJ}}\text{ cm}^{-3}. \tag{25}$$

The Coulomb coupling parameter $\Gamma_+ = e^2/\left(a\langle T_+\rangle_\gamma\right)$, where the ion-sphere radius $a = (4\pi n_+/3)^{-1/3}$ expresses the ratio of Coulomb energy of the particles to their thermal energy. This parameter is much less than unity,

$$\Gamma_+ = 5 \times 10^{-8}\left(n_+/10^{16}\text{ cm}^{-3}\right)^{1/3}\left(\langle T_+\rangle_\gamma/1\text{ MeV}\right)^{-1} \ll 1,$$

because the particles are dilute and their temperature is high. The number of particles in a Debye sphere $N_{\text{D}} = (3\Gamma_+)^{-3/2}$ is correspondingly high,

$$N_{\text{D}} = 1.7 \times 10^{10}\left(n_+/10^{16}\text{ cm}^{-3}\right)^{-1/2}\left(\langle T_+\rangle_\gamma/1\text{ MeV}\right)^{3/2}.$$

The expanding cloud may appear to be a classical weakly coupled plasma.[54] For collective excitation to be supported, however, the cloud size must exceed the Debye length,

$$\lambda_{\text{D}} = \sqrt{4\pi n_+ e^2/\langle T_+\rangle_\gamma} \approx 7.4 \times 10^3 \times \left(n_+/10^{16}\text{ cm}^{-3}\right)^{-1/2}\left(\langle T_+\rangle_\gamma/1\text{ MeV}\right)^{1/2}\text{ cm}.$$

The ratio of density scale length $L_n = \left|\text{d}\log n_+/\text{d}r\right|^{-1}$ to the Debye length, for the expansion given by Eq. (23), is

$$\frac{L_n}{\lambda_{\text{D}}} = \frac{1}{2}\left(\frac{\dot{Y}_{+,\gamma}e^2}{c\langle T_+\rangle_\gamma}\right)^{1/2}. \tag{26}$$

This ratio is independent of r, assuming that the expansion is isothermal,

$$\frac{L_n}{\lambda_{\text{D}}} = 1.7\left(\frac{\dot{Y}_{+,\gamma}}{10^{12}\text{ ps}^{-1}\text{ kJ}^{-1}}\right)^{1/2}\left(\frac{E_{\text{hot}}}{2.5\text{ kJ}}\right)^{1/2}\left(\frac{\langle T_+\rangle_\gamma}{1\text{ MeV}}\right)^{-1/2}. \tag{27}$$

Adiabatic expansion would give a more favorable ratio for larger radii.

From the above estimate [Eq. (27)], the rate of positron production $\dot{Y}_{+,\gamma}$ is probably insufficient to guarantee the production of a pair plasma for laser energies of several kJ. The chances for success can be greatly improved, however, by limiting the expansion of the cloud.

Confinement of the pairs, such as might be obtained in a magnetic mirror,[10] is not necessary. Radial confinement of the order of 100 μm with free expansion in the remaining dimension will lead to a cloud that is several tens of Debye lengths in size[55]

[(d)] Electrostatic sheath fields and large-scale, self-generated dc magnetic fields will modify the expansion.

and has many particles in a Debye sphere; i.e., the cloud will form a classical weakly coupled plasma. Radial confinement may be obtained in several ways, e.g., by using one of the OMEGA EP beams to magnetize the positron-generation foil using a "magnetic trap" target,[55] or by the application of an externally generated magnetic field of the type used in the Magneto-Inertial Fusion Electrical Discharge System (MIFEDS).[56]

Summary

The yield of electron–positron pairs caused by both direct and indirect processes resulting from the interaction of laser-accelerated hot electrons with target atoms has been calculated. Indirect production is the dominant process for practical target interaction conditions.

Calculation of the indirect yield required two steps: First, an expression for the hard x-ray spectrum and yield was obtained [Eqs. (9) and (10)]. This was computed in the limit in which the majority of fast electrons are confined to the target by space-charge effects (the so-called "refluxing limit"). Second, convenient expressions were obtained for the pair spectrum [Eq. (21)] and pair yield [Eq. (22)]. These are given in terms of the photon spectrum $N_\gamma(k)$ and an angle-average effective depth for photons $\langle \rho L \rangle_\Omega$, which is dependent on the photon energy and target geometry [Eqs. (17–20)]. Predictions of bremsstrahlung yield [Eq. (10)] and spectrum [Eq. (9)] are experimentally verifiable and might prove useful for other applications.

For a given target thickness, the efficiency of pair creation (pairs per kJ of hot electrons) was shown to increase with the temperature Θ_{hot} of the laser-excited electrons, with maximum production efficiency obtained at a hot-electron temperature of $\Theta_{hot} = 50$ MeV. Energetic efficiencies of $\sim 1.6 \times 10^{-4}$ are shown to be achievable at $\Theta_{hot} = 2$ MeV. The corresponding laser intensity for optimal yield could optimistically be as low as $I_L \sim 10^{22}$ W/cm^2.

The optimal "useful" yield is limited by the range of the pairs in the target material. It has been maximized by matching the target thickness to the expected penetration distance of the pairs as a function of laser intensity and Θ_{hot} scaling (see Fig. 116.5). It was demonstrated that a yield of $Y_{+,\gamma} = 5 \times 10^{11}$ pairs might be generated on OMEGA EP, provided that the hot-electron temperature is consistent with the ponderomotive scaling. More unfavorable yields are obtained with Beg scaling.

Pair-production rates were calculated and shown to have a very broad maximum of $\dot{Y}_{+,\gamma} = 1 \times 10^{24}\ s^{-1}\ kJ^{-1}$, obtained at $I_L = 1.5 \times 10^{21}$ W/cm^2 ($\Theta_{hot} = 16.4$ MeV), which is a significantly lower Θ_{hot} than that required for maximizing the yield. The rate displays little sensitivity to the hot-electron temperature over a wide range. This implies that, as far as production rates are concerned, increasing laser intensities above the currently attainable levels is less important than increasing available laser energy, which does not rely on further technological advances.

An estimate of plasma parameters, assuming free expansion of the pairs into the vacuum, indicates that current kJ-class, high-intensity lasers may come close to producing a pair plasma with a physical size similar to, or slightly smaller than, the Debye length. A successful demonstration will probably require efforts to confine or limit the expansion of the expanding pairs. Possible confinement schemes, such as externally applied magnetic fields, are suggested. The yields, production rates, and energy spectra that have been computed in this article will be useful for particle-in-cell (PIC) or implicit-hybrid PIC calculations of the dynamics of expansion and pair-plasma production.

ACKNOWLEDGMENT

This work was supported by the U.S. Department of Energy Office of Inertial Confinement Fusion under Cooperative Agreement No. DE-FC52-08NA28302, the University of Rochester, and the New York State Energy Research and Development Authority. The support of DOE does not constitute an endorsement by DOE of the views expressed in this article.

REFERENCES

1. V. Tsytovich and C. B. Wharton, Comments Plasma Phys. Control. Fusion **4**, 91 (1978).
2. G. P. Zank and R. G. Greaves, Phys. Rev. E **51**, 6079 (1995).
3. M. L. Burns, A. K. Harding, and R. Ramaty, eds. *Positron-Electron Pairs in Astrophysics, AIP Conference Proceedings 101* (American Institute of Physics, New York, 1983).
4. B. A. Remington *et al.*, Science **284**, 1488 (1999).
5. C. M. Surko, M. Leventhal, and A. Passner, Phys. Rev. Lett. **62**, 901 (1989).
6. C. M. Surko and T. J. Murphy, Phys. Fluids B **2**, 1372 (1990).
7. T. Kurihara *et al.*, Nucl. Instrum. Methods Phys. Res. B **171**, 164 (2000).
8. C. M. Surko *et al.*, Nucl. Instrum. Methods Phys. Res. B **171**, 2 (2000).
9. T. S. Pedersen *et al.*, J. Phys. B **36**, 1029 (2003).
10. G. Gibson, W. C. Jordan, and E. J. Lauer, Phys. Rev. Lett. **5**, 141 (1960).
11. J. W. Shearer *et al.*, Phys. Rev. A **8**, 1582 (1973).

12. E. P. Liang, S. C. Wilks, and M. Tabak, Phys. Rev. Lett. **81**, 4887 (1998).
13. D. A. Gryaznykh, Ya. Z. Kandiev, and V. A. Lykov, JETP Lett. **67**, 257 (1998).
14. T. E. Cowan *et al.*, in *High-Field Science*, edited by T. Tajima, K. Mima, and H. Baldis (Kluwer Academic, New York, 2000), pp. 145–156.
15. C. Gahn *et al.*, Appl. Phys. Lett. **77**, 2662 (2000).
16. K. Nakashima and H. Takabe, Phys. Plasmas **9**, 1505 (2002).
17. S. C. Wilks *et al.*, Astrophys. Space Sci. **298**, 347 (2005).
18. L. J. Waxer, D. N. Maywar, J. H. Kelly, T. J. Kessler, B. E. Kruschwitz, S. J. Loucks, R. L. McCrory, D. D. Meyerhofer, S. F. B. Morse, C. Stoeckl, and J. D. Zuegel, Opt. Photonics News **16**, 30 (2005).
19. M. H. Key, Phys. Plasmas **14**, 055502 (2007).
20. J. Schwinger, Phys. Rev. **82**, 664 (1951).
21. E. Brezin and C. Itzykson, Phys. Rev. D **2**, 1191 (1970).
22. H. Nitta *et al.*, Phys. Rev. Lett. **93**, 180407 (2004).
23. S. P. Hatchett, C. G. Brown, T. E. Cowan, E. A. Henry, J. S. Johnson, M. H. Key, J. A. Koch, A. B. Langdon, B. F. Lasinski, R. W. Lee, A. J. MacKinnon, D. M. Pennington, M. D. Perry, T. W. Phillips, M. Roth, T. C. Sangster, M. S. Singh, R. A. Snavely, M. A. Stoyer, S. C. Wilks, and K. Yasuike, Phys. Plasmas **7**, 2076 (2000).
24. S. C. Wilks *et al.*, Phys. Rev. Lett. **69**, 1383 (1992).
25. F. N. Beg *et al.*, Phys. Plasmas **4**, 447 (1997).
26. M. G. Haines, Imperial College, private communications (2008).
27. T. E. Cowan, M. Roth, J. Johnson, C. Brown, M. Christl, W. Fountain, S. Hatchett, E. A. Henry, A. W. Hunt, M. H. Key, A. MacKinnon, T. Parnell, D. M. Pennington, M. D. Perry, T. W. Phillips, T. C. Sangster, M. Singh, R. Snavely, M. Stoyer, Y. Takahashi, S. C. Wilks, and K. Yasuike, Nucl. Instrum. Methods Phys. Res. A **455**, 130 (2000).
28. H. Chen *et al.*, Rev. Sci. Instrum. **77**, 10E703 (2006).
29. H. J. Bhabha, Proc. R. Soc. Lond. A, Math. Phys. Sci. **152**, 559 (1935).
30. Y.-S. Tsai, Rev. Mod. Phys. **46**, 815 (1974).
31. G. Racah, Nuovo Cimento **14**, 93 (1937).
32. B. B. Rossi, *High-Energy Particles*, Prentice-Hall Physics Series (Prentice-Hall, New York, 1952).
33. T. Murota, A. Ueda, and H. Tanaka, Prog. Theor. Phys. **16**, 482 (1956).
34. D. A. Gryaznykh, Phys. At. Nucl. **61**, 394 (1998).
35. V. N. Baĭer and V. S. Fadin, Sov. Phys.-JETP **34**, 253 (1972).
36. J. Myatt, W. Theobald, J. A. Delettrez, C. Stoeckl, M. Storm, T. C. Sangster, A. V. Maximov, and R. W. Short, Phys. Plasmas **14**, 056301 (2007).
37. P. M. Nilson, W. Theobald, J. F. Myatt, C. Stoeckl, M. Storm, J. D. Zuegel, R. Betti, D. D. Meyerhofer, and T. C. Sangster, "Bulk Heating of Dense Plasma High-Intensity Laser-Plasma Interactions," submitted to Physical Review E.
38. H. O. Wyckoff, *ICRU Report*, **37**, International Commission on Radiation Units and Measurements, Inc., Bethesda, MD (1984).
39. H. W. Koch and J. W. Motz, Rev. Mod. Phys. **31**, 920 (1959).
40. H. A. Bethe and J. Ashkin, in *Experimental Nuclear Physics*, edited by E. Sergrè (Wiley, New York, 1953), Vol. I, pp. 166–357.
41. S. M. Seltzer and M. J. Berger, Nucl. Instrum. Methods Phys. Res. B **12**, 95 (1985).
42. J. H. Hubbell, H. A. Gimm, and I. Øverbø, J. Phys. Chem. Ref. Data **9**, 1023 (1980).
43. S. D. Baton *et al.*, High Energy Density Phys. **3**, 358 (2007).
44. M. Tabak, Bull. Am. Phys. Soc. **52**, 284 (2007).
45. M. Abramowitz and I. A. Stegun, eds. *Handbook of Mathematical Functions with Formulas, Graphs, and Mathematical Tables*, Applied Mathematics Series 55 (U.S. Government Printing Office, Washington, DC, 1964).
46. J. D. Bjorken and S. D. Drell, *Relativistic Quantum Mechanics*, International Series in Pure and Applied Physics (McGraw-Hill, New York, 1964).
47. P. J. Ebert, A. F. Lauzon, and E. M. Lent, Phys. Rev. **183**, 422 (1969).
48. T. Tabata, R. Ito, and S. Okabe, Nucl. Instrum. Methods **103**, 85 (1972).
49. N. G. Basov, S. Yu. Gus'kov, and L. P. Feokistov, J. Sov. Laser Res. **13**, 396 (1992).
50. M. Tabak *et al.*, Phys. Plasmas **1**, 1626 (1994).
51. P. M. Nilson, W. Theobald, J. Myatt, C. Stoeckl, M. Storm, O. V. Gotchev, J. D. Zuegel, R. Betti, D. D. Meyerhofer, and T. C. Sangster, Phys. Plasmas **15**, 056308 (2008).
52. M. Dunne, Nat. Phys. **2**, 2 (2006).
53. S. Atzeni *et al.*, Phys. Plasmas **15**, 056311 (2008).
54. S. Ichimaru, *Statistical Plasma Physics. Volume I, Basic Principles*, Frontiers in Physics (Addison-Wesley, Redwood City, CA, 1992).
55. J. Myatt, A. V. Maximov, R. W. Short, and D. D. Meyerhofer, Bull. Am. Phys. Soc. **52**, 66 (2007).
56. O. V. Gotchev, N. W. Jang, J. P. Knauer, M. D. Barbero, R. Betti, C. K. Li, and R. D. Petrasso, J. Fusion Energy **27**, 25 (2008).